

CG dinucleotide suppression enables antiviral defence targeting non-self RNA

Matthew A. Takata¹, Daniel Gonçalves-Carneiro¹, Trinity M. Zang^{1,2}, Steven J. Soll^{1,2}, Ashley York¹, Daniel Blanco-Melo¹ & Paul D. Bieniasz^{1,2}

Vertebrate genomes exhibit marked CG suppression—that is, lower than expected numbers of 5'-CG-3' dinucleotides¹. This feature is likely to be due to C-to-T mutations that have accumulated over hundreds of millions of years, driven by CG-specific DNA methyl transferases and spontaneous methyl-cytosine deamination. Many RNA viruses of vertebrates that are not substrates for DNA methyl transferases mimic the CG suppression of their hosts^{2–4}. This property of viral genomes is unexplained^{4–6}. Here we show, using synonymous mutagenesis, that CG suppression is essential for HIV-1 replication. The deleterious effect of CG dinucleotides on HIV-1 replication was cumulative, associated with cytoplasmic RNA depletion, and was exerted by CG dinucleotides in both translated and non-translated exonic RNA sequences. A focused screen using small inhibitory RNAs revealed that zinc-finger antiviral protein (ZAP)⁷ inhibited virion production by cells infected with CG-enriched HIV-1. Crucially, HIV-1 mutants containing segments whose CG content mimicked random nucleotide sequence were defective in unmanipulated cells, but replicated normally in ZAP-deficient cells. Crosslinking-immunoprecipitation-sequencing assays demonstrated that ZAP binds directly and selectively to RNA sequences containing CG dinucleotides. These findings suggest that ZAP exploits host CG suppression to identify non-self RNA. The dinucleotide composition of HIV-1, and perhaps other RNA viruses, appears to have adapted to evade this host defence.

To identify *cis*-acting RNA elements within the HIV-1 genome that are important for its replication, we generated a mutant HIV-1 sequence containing the maximum number of synonymous mutations in open reading frames (ORFs). Blocks of mutations (mean of around 125 mutations per block) were represented in 16 proviral plasmids (A–P) containing a *gfp* reporter (Fig. 1a). Mutant viruses were divided into three groups, depending on their replication properties. Group 1 mutants displayed near-normal viral replication and group 2 mutants were defective, exhibiting severe splicing defects (unpublished observations). Group 3 mutants yielded near-normal infectious titres when proviral plasmids were transfected into 293T cells and lacked an obvious splicing defect, but were defective in spreading replication assays (Fig. 1b, c, Extended Data Fig. 1a).

Mapping experiments that used derivatives of the defective group 3 mutant viruses L and M that contained mutated segments in *env* revealed that the replication defects of these viruses were not caused by perturbation of a single discrete element. Indeed, mutants LC, LD, LE, LF, MA, MC and MD, which contained smaller mutant segments, collectively representing all mutations in L and M, each replicated with kinetics close to those of wild-type HIV-1 (HIV-1_{WT}) (Fig. 1a–d). Moreover, when the mutations in four replication-competent *pol* mutants (E–H, Fig. 1a) were combined, the resulting mutant virus (EH) was defective (Fig. 1e). Thus, HIV-1 replication defects were induced by cumulative effects of synonymous mutations in *pol* or *env*.

The HIV-1 genome is sparse in C mononucleotides⁸ and, like many vertebrate viruses^{2–4}, is particularly deficient in CG dinucleotides,

(Fig. 1f). Our synonymous mutagenesis coincidentally increased the CG dinucleotide content in mutant segments to a level similar to that of random sequence (Fig. 1f). We generated derivatives of mutant L, termed L_{CG} and L_{OTH}, respectively, containing only mutations that generated new CG dinucleotides (37 of 145 original mutations) or the 108 other mutations (Supplementary Data 1). We also generated mutants that maximized the CG or, as a further control, GC dinucleotide content in the same segment (L_{CG-HI} and L_{GC-HI}) (Extended Data Table 1). These proviral plasmids each yielded similar levels of infectious virus following transfection of 293T cells

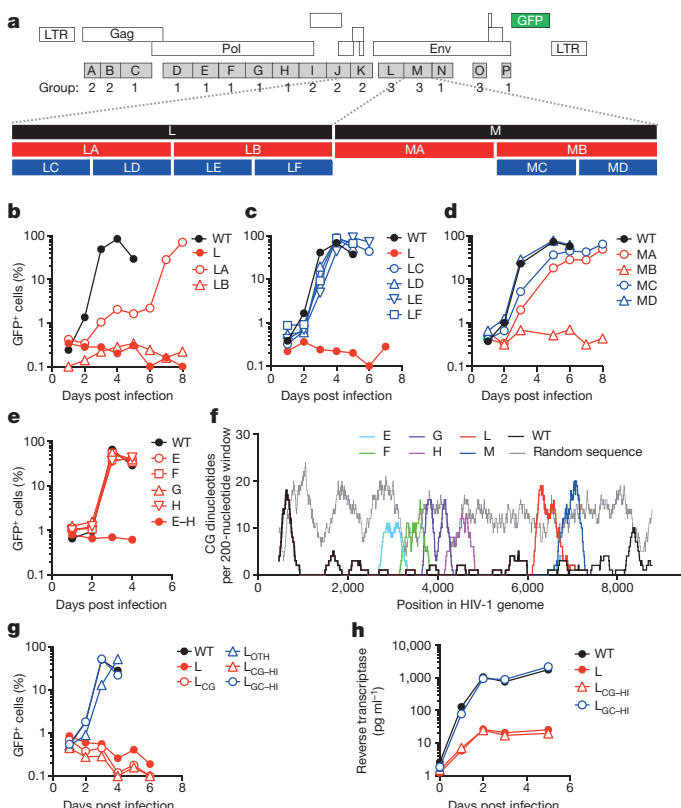


Figure 1 | Synonymous mutagenesis reveals inhibitory effects of CG dinucleotides on HIV-1 replication. **a**, Representation of HIV-1_{NHG}, a human immunodeficiency virus type-1 provirus encoding *gfp* in place of *nef*, indicating synonymous mutant blocks, and corresponding phenotypes (see text). **b–e**, Replication of HIV-1 mutants in MT4 cells, as measured by fluorescence-activated cell sorting (FACS) enumeration of infected cells. **f**, Number of CG dinucleotides in a 200-nucleotide sliding window in viral and random sequences. **g**, Replication of HIV-1 mutants in MT4 cells, measured as in **b**. **h**, Replication of HIV-1 mutants in primary lymphocytes, measured by supernatant reverse transcriptase activity.

¹Laboratory of Retrovirology, The Rockefeller University, New York, New York, USA. ²Howard Hughes Medical Institute, The Rockefeller University, New York, New York, USA.

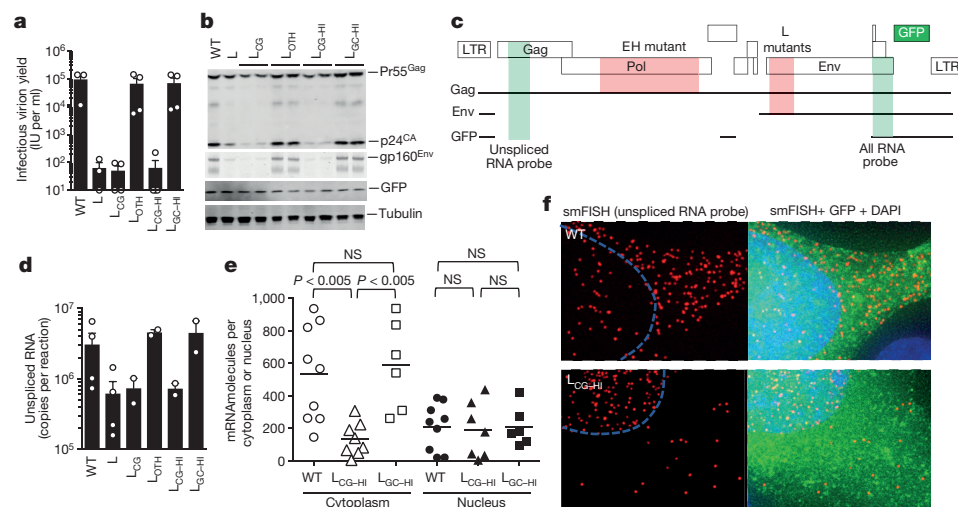


Figure 2 | CG dinucleotides cause depletion of cytoplasmic RNA.

a, Single-cycle infectious virus yield, following infection of MT4 cells with equal titres of HIV-1_{WT} and mutants (mean \pm s.e.m., $n = 3$ independent experiments). b, Western blot analysis 48 h after a single-cycle infection of MT4 cells with wild-type or mutant HIV-1, representative of three experiments. c, Location of salient exons (black lines), mutated segments (red shading) and smFISH probes (green shading) in HIV-1 mRNAs. d, RT-qPCR quantification of unspliced RNA in MT4 cells in a single-cycle infection assay (mean \pm s.e.m., $n = 2$ or 4 independent experiments).

(Extended Data Fig. 1a). However, L_{CG} and L_{CG-HI} were defective in MT4 cells, whereas L_{OTH} and L_{GC-HI} replicated with kinetics close to those of HIV-1_{WT} (Fig. 1g). Mutants L and L_{CG-HI} also replicated at about 100-fold lower levels than HIV-1_{WT} and L_{GC-HI} in primary lymphocytes (Fig. 1h, Extended Data Fig. 1b, c). Thus, suppression of CG but not GC dinucleotides appears to be essential for HIV-1 replication.

To understand the basis of replication defects in the CG-enriched HIV-1 mutants, we infected MT4 cells with equal titres of each virus in single-cycle replication experiments. Notably, cells infected with L, L_{CG} or L_{CG-HI} generated about 1,000-fold fewer infectious progeny virions than did cells infected with L_{OTH} or L_{GC-HI} (Fig. 2a). Infectious virion yields from EH-infected cells were similarly reduced (Extended Data Fig. 2a). Western blot analyses revealed reduced levels of viral Gag and Env proteins in cells infected with L, L_{CG} or L_{CG-HI}, but the same levels as HIV-1_{WT} for cells infected with L_{OTH} or L_{GC-HI} (Fig. 2b). Expression of the *gfp* reporter that was embedded in the *nef* gene, and therefore expressed via an mRNA from which the L segment is removed by splicing (Fig. 2c), was equivalent for each virus (Fig. 2b, Extended Data Fig. 2b). A deficit in Gag protein levels also occurred in EH-infected cells. However, these cells generated normal levels of both Env and GFP proteins, whose spliced mRNAs lack the CG-enriched EH segment (Extended Data Fig. 2c).

Unspliced viral RNA levels in single-cycle infected MT4 cells, measured by reverse transcription-quantitative PCR (RT-qPCR), were five-to-tenfold lower in cells infected with L, L_{CG}, L_{CG-HI} or EH but at HIV-1_{WT} levels in cells infected with L_{OTH}, L_{GC-HI}, E, F, G or H (Fig. 2d, Extended Data Fig. 2d). Single-molecule fluorescence *in situ* hybridization (smFISH) experiments using a *gag* probe revealed that the deficit in unspliced viral RNA occurred specifically in the cytoplasm in L_{CG-HI}-infected cells, whereas levels of unspliced RNA in the nucleus were equivalent for HIV-1_{WT}, L_{CG-HI} and L_{GC-HI} (Fig. 2e, f, Extended Data Fig. 3). Similar smFISH experiments using a probe that detected all spliced and unspliced viral RNAs (Fig. 2c) revealed a marginal, statistically ambiguous deficit for cells infected with L_{CG-HI} (Extended Data Figs 2e, 4). Thus, incompletely spliced RNAs (which represent only a subset of total HIV-1 RNAs)⁹ appeared to be selectively depleted in L_{CG-HI}-infected cells.

e, Quantification of unspliced RNA (fluorescent spots) by smFISH in cytoplasm and nucleus of infected HOS/CXCR4-CD4 cells. Each symbol represents an individual cell nucleus or cytoplasm. Horizontal lines show mean. *P* values determined using Mann-Whitney test, $n = 6$, 8 or 9 individual cells. NS, not significant. f, Examples of smFISH analysis of cells infected with HIV-1_{WT} or mutant HIV (red, smFISH *gag* probe; green, GFP; blue, Hoechst dye). Blue line indicates nucleus-cytoplasm boundary. Representative of three independent experiments.

Because a deficit in levels of CG-containing RNAs and their protein products was the foundational defect in cells infected with the defective viral mutants, we conducted a focused small inhibitory RNA (siRNA) screen targeting proteins involved in RNA degradation pathways (for example, the microRNA, nonsense-mediated decay and RNA exosome pathways) (Fig. 3a, Extended Data Fig. 5a). Single-cycle replication experiments revealed that knockdown of ZAP⁷ almost completely restored infectious virion yield from L_{CG-HI}-infected cells (Fig. 3a). Knockdown of TRIM25, which enhances ZAP activity^{10,11}, also increased viral yield.

We generated ZAP^{-/-} MT4 cells lacking both major ZAP isoforms (ZAP-L and ZAP-S, Fig. 3b) using CRISPR-Cas9 genome editing. While previous work has indicated that an overexpressed ZAP fragment can inhibit HIV-1 infection¹², knockout of endogenous ZAP in MT4 cells did not affect HIV-1_{WT} or L_{CG-HI} replication (Fig. 3c). Strikingly, L_{CG-HI} and EH, which were defective in unmanipulated MT4 cells, replicated with kinetics that were indistinguishable from those of HIV-1_{WT} in ZAP^{-/-} MT4 cells (Fig. 3c). The deficits in viral protein levels observed in cells infected with CG-enriched viruses were abolished in ZAP^{-/-} cells (Fig. 3d). Reconstitution of ZAP^{-/-} MT4 cells with a CRISPR-resistant, doxycycline-inducible ZAP-S construct (ZAP_{DI}) enabled doxycycline-dependent inhibition of CG-enriched virus replication and protein expression in single-cycle assays, but did not affect HIV-1_{WT} (Fig. 3c, Extended Data Fig. 5b, c). Moreover, the deficit in unspliced viral RNA seen in cells infected with CG-enriched viruses was abolished in ZAP^{-/-} cells and reinstated in a doxycycline-dependent manner in ZAP_{DI}-reconstituted ZAP^{-/-} cells (Fig. 3e).

We transferred the L-mutant segment and its derivatives into the 3' UTR of a reporter construct encoding a synthetic CG-depleted *fluc* gene (Extended Data Fig. 6a). The CG-enriched L-derived elements inhibited luciferase expression approximately fivefold in this context in a simple plasmid transfection assay (Fig. 3f). These inhibitory effects were abolished when ZAP^{-/-} HeLa cells were transfected (Fig. 3f, Extended Data Fig. 6b). Elevating the CG dinucleotide content of fragments from naturally CG-suppressed vesicular stomatitis virus or influenza virus-derived RNA sequences^{4,5} (Extended Data Fig. 6a, c) conferred sensitivity to ZAP-L in cotransfection assays with similar reporter constructs (Extended Data Fig. 6d).

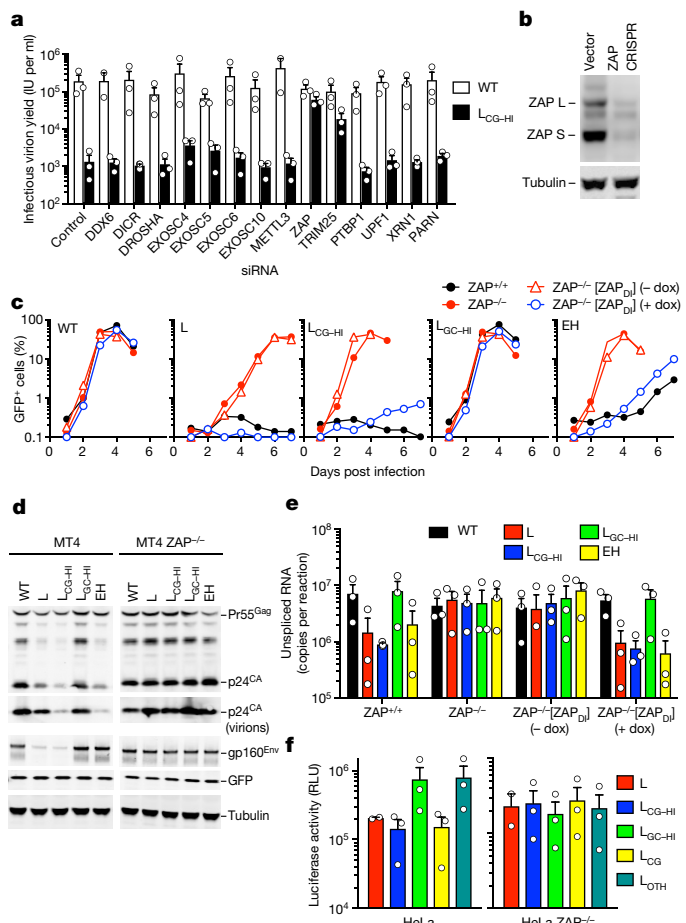


Figure 3 | ZAP specifically inhibits CG-enriched HIV-1 replication. **a**, Single-cycle infectious HIV-1_{WT} and L_{CG-HI} yield from siRNA-transfected HeLa cells (mean \pm s.e.m., $n = 3$ independent experiments). **b**, Western blot analysis of MT4 cells following CRISPR mutation of ZAP exon 1. Representative of three experiments. **c**, Replication of HIV-1 mutants in ZAP^{+/+}, ZAP^{-/-} and doxycycline-inducible ZAP (ZAP_{Dl})-reconstituted ZAP^{-/-} MT4 cells, as measured by FACS enumeration of infected cells. **d**, Western blot analysis of cells and virions 48 h after a single-cycle infection of ZAP^{+/+} and ZAP^{-/-} MT4 cells with WT and mutant HIV-1. **e**, RT-qPCR quantification of unspliced RNA in MT4 cells in a single-cycle infection assay (mean \pm s.e.m., $n = 3$ independent experiments). **f**, Luciferase expression following transfection of HeLa or HeLa ZAP^{-/-} cells with reporter plasmids incorporating HIV-1 RNA segments as 3' UTRs (mean \pm s.e.m., $n = 3$ independent experiments).

ZAP has been reported to bind RNA, but no shared features of its target sequences are evident^{13–16}. To determine the RNA binding specificity of ZAP, we used crosslinking-immunoprecipitation-sequencing (CLIP-seq) assays in cells infected with HIV-1_{WT} or mutant L. Remarkably, ZAP bound to the HIV-1 genome predominantly at the precise location of the CG-enriched segment in mutant L (Fig. 4a, b). Conversely, ZAP bound less frequently to HIV-1_{WT} and the unaltered portions of the L genome. Infrequent ZAP binding sites in the HIV-1 genome almost always coincided with rare CG dinucleotides (Fig. 4a, Extended Data Fig. 7a).

Although the L mutant genome was the single most frequently bound RNA in infected cells, ZAP also bound cellular mRNAs (Extended Data Fig. 7b). CG suppression is marked in human mRNA ORF and 3' UTR sequences¹ but was absent in the subset of these sequences that represented preferred ZAP binding sites (Extended Data Fig. 7c–e). A more detailed analysis of dinucleotides that are underrepresented (CG and UA) or overrepresented (UG) in ORFs and 3' UTRs as well as an inverted control dinucleotide (GC) revealed that ZAP binding sites

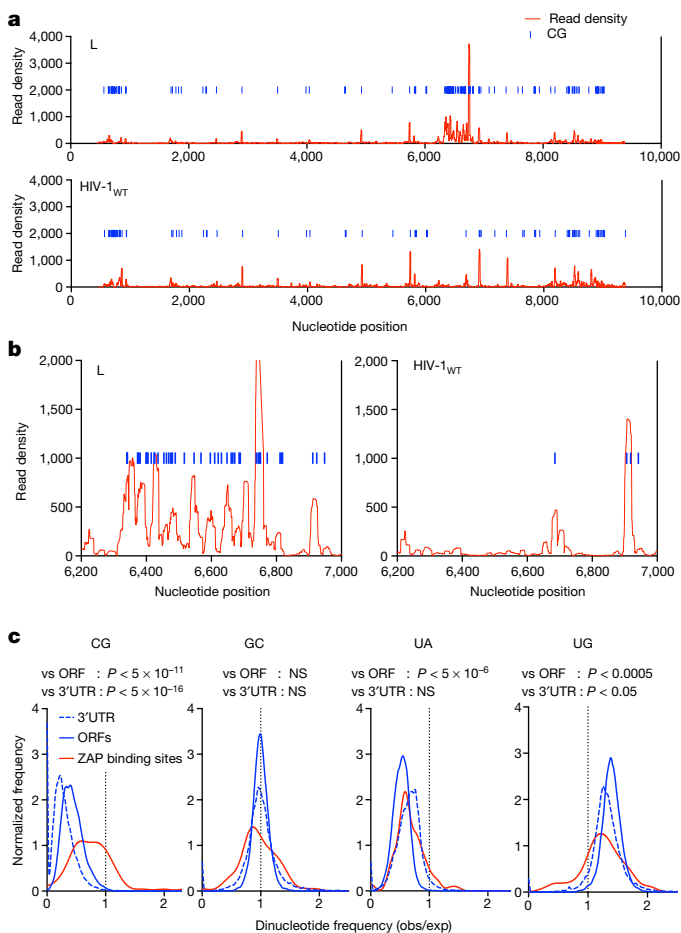


Figure 4 | ZAP binds directly and preferentially to CG dinucleotide-containing RNA. **a**, CLIP analysis of the frequency with which L mutant and HIV-1_{WT} RNA sequences are bound to ZAP in infected cells, versus their position in the viral genome. CG dinucleotides are indicated as blue lines. The L mutant segment occupies positions 6,307 to 6,805. **b**, Expanded views of the L portion of the CLIP graphs in a. **c**, Frequency distributions of CG, GC, UA and UG dinucleotide observed/expected frequencies in human ORFs, 3' UTRs and the top 100 ZAP-binding sites. P values for ZAP binding sites ($n = 100$) versus ORFs ($n = 35,170$) or 3' UTRs ($n = 135,557$) calculated using Welch's unequal variance t -tests.

were highly CG-enriched (Fig. 4c, Extended Data Fig. 7f). Conversely, UA, UG or GC dinucleotides were present in preferred ZAP binding elements at frequencies similar to those of ORFs and 3' UTRs (Fig. 4c). A control RNA binding protein (APOBEC3G) showed no preference for CG-enriched elements (Extended Data Fig. 7g).

The replication of several, but not all, RNA and reverse-transcribing viruses is inhibited by overexpressed or endogenous ZAP^{7,12,14,17–24}. Inspection of the dinucleotide composition of these viral genomes revealed that the degree of CG suppression generally predicted ZAP resistance (Extended Data Fig. 8a). Moreover, the degree to which previously mapped viral RNA elements conferred sensitivity to ZAP in reporter assays was also generally predicted by the product of their length and the degree to which CG nucleotides were suppressed (Extended Data Fig. 8b).

CG suppression in ORFs is synonymous with codon-pair bias^{6,25–27}. However, the CG- and ZAP-dependent inhibition of HIV-1 protein expression occurred when CG-enriched elements were incorporated into exonic (but not intronic) translated or 3' UTR portions of the corresponding pre-mRNAs. Thus, CG dinucleotides exert effects post-transcriptionally but independent of codon-pair translation efficiency. Rather, direct ZAP recognition causes cytoplasmic depletion of RNAs with high CG content. While ZAP can also regulate the levels

of certain host mRNAs (for example, that encoding TRAILR4)²⁸, this activity requires the C-terminal poly ADP ribose polymerase (PARP) domain that is absent in ZAP-S (which exhibits antiviral activity). Most cellular mRNAs are unaffected by ZAP²⁸. Thus, it appears that the main targets of ZAP are non-self, viral RNAs in which CG suppression is incomplete. Manipulation of the CG content in viruses^{25,26} and manipulation of ZAP in cells could enable levels of viral attenuation or recombinant gene expression to be adjusted, with many possible applications.

Online Content Methods, along with any additional Extended Data display items and Source Data, are available in the online version of the paper; references unique to these sections appear only in the online paper.

Received 24 May; accepted 30 August 2017.

Published online 27 September 2017.

1. Karlin, S. & Mrázek, J. Compositional differences within and between eukaryotic genomes. *Proc. Natl Acad. Sci. USA* **94**, 10227–10232 (1997).
2. Karlin, S., Doerfler, W. & Cardon, L. R. Why is CpG suppressed in the genomes of virtually all small eukaryotic viruses but not in those of large eukaryotic viruses? *J. Virol.* **68**, 2889–2897 (1994).
3. Rima, B. K. & McMullan, N. V. Dinucleotide and stop codon frequencies in single-stranded RNA viruses. *J. Gen. Virol.* **78**, 2859–2870 (1997).
4. Greenbaum, B. D., Levine, A. J., Bhanot, G. & Rabadan, R. Patterns of evolution and host gene mimicry in influenza and other RNA viruses. *PLoS Pathog.* **4**, e1000079 (2008).
5. Cheng, X. et al. CpG usage in RNA viruses: data and hypotheses. *PLoS One* **8**, e74109 (2013).
6. Futcher, B. et al. Reply to Simmonds et al.: Codon pair and dinucleotide bias have not been functionally distinguished. *Proc. Natl Acad. Sci. USA* **112**, E3635–E3636 (2015).
7. Gao, G., Guo, X. & Goff, S. P. Inhibition of retroviral RNA production by ZAP, a CCCH-type zinc finger protein. *Science* **297**, 1703–1706 (2002).
8. van Hemert, F., van der Kuy, A. C. & Berkhouit, B. On the nucleotide composition and structure of retroviral RNA genomes. *Virus Res.* **193**, 16–23 (2014).
9. Karn, J. & Stoltzfus, C. M. Transcriptional and posttranscriptional regulation of HIV-1 gene expression. *Cold Spring Harb. Perspect. Med.* **2**, a006916 (2012).
10. Li, M. M. et al. TRIM25 enhances the antiviral action of zinc-finger antiviral protein (ZAP). *PLoS Pathog.* **13**, e1006145 (2017).
11. Zheng, X. et al. TRIM25 is required for the antiviral activity of zinc finger antiviral protein. *J. Virol.* **91**, e00088–17 (2017).
12. Zhu, Y. et al. Zinc-finger antiviral protein inhibits HIV-1 infection by selectively targeting multiply spliced viral mRNAs for degradation. *Proc. Natl Acad. Sci. USA* **108**, 15834–15839 (2011).
13. Guo, X., Carroll, J. W., Macdonald, M. R., Goff, S. P. & Gao, G. The zinc finger antiviral protein directly binds to specific viral mRNAs through the CCCH zinc finger motifs. *J. Virol.* **78**, 12781–12787 (2004).
14. Zhu, Y. & Gao, G. ZAP-mediated mRNA degradation. *RNA Biol.* **5**, 65–67 (2008).
15. Chen, S. et al. Structure of N-terminal domain of ZAP indicates how a zinc-finger protein recognizes complex RNA. *Nat. Struct. Mol. Biol.* **19**, 430–435 (2012).
16. Huang, Z., Wang, X. & Gao, G. Analyses of SELEX-derived ZAP-binding RNA aptamers suggest that the binding specificity is determined by both structure and sequence of the RNA. *Protein Cell* **1**, 752–759 (2010).
17. Bick, M. J. et al. Expression of the zinc-finger antiviral protein inhibits alphavirus replication. *J. Virol.* **77**, 11555–11562 (2003).
18. Müller, S. et al. Inhibition of filovirus replication by the zinc finger antiviral protein. *J. Virol.* **81**, 2391–2400 (2007).
19. Mao, R. et al. Inhibition of hepatitis B virus replication by the host zinc finger antiviral protein. *PLoS Pathog.* **9**, e1003494 (2013).
20. Lin, Y. et al. Identification and characterization of alphavirus M1 as a selective oncolytic virus targeting ZAP-defective human cancers. *Proc. Natl Acad. Sci. USA* **111**, E4504–E4512 (2014).
21. Goodier, J. L., Pereira, G. C., Cheung, L. E., Rose, R. J. & Kazazian, H. H., Jr. The broad-spectrum antiviral protein ZAP restricts human retrotransposition. *PLoS Genet.* **11**, e1005252 (2015).
22. Moldovan, J. B. & Moran, J. V. The zinc-finger antiviral protein ZAP inhibits LINE and Alu retrotransposition. *PLoS Genet.* **11**, e1005121 (2015).
23. Liu, C. H., Zhou, L., Chen, G. & Krug, R. M. Battle between influenza A virus and a newly identified antiviral activity of the PARP-containing ZAPL protein. *Proc. Natl Acad. Sci. USA* **112**, 14048–14053 (2015).
24. Tang, Q., Wang, X. & Gao, G. The short form of the zinc finger antiviral protein inhibits influenza A virus protein expression and is antagonized by the virus-encoded NS1. *J. Virol.* **91**, e01909–16 (2017).
25. Coleman, J. R. et al. Virus attenuation by genome-scale changes in codon pair bias. *Science* **320**, 1784–1787 (2008).
26. Tulloch, F., Atkinson, N. J., Evans, D. J., Ryan, M. D. & Simmonds, P. RNA virus attenuation by codon pair deoptimisation is an artefact of increases in CpG/UpA dinucleotide frequencies. *eLife* **3**, e04531 (2014).
27. Kunec, D. & Osterrieder, N. Codon pair bias is a direct consequence of dinucleotide bias. *Cell Reports* **14**, 55–67 (2016).
28. Todorova, T., Bock, F. J. & Chang, P. PARP13 regulates cellular mRNA post-transcriptionally and functions as a pro-apoptotic factor by destabilizing TRAILR4 transcript. *Nat. Commun.* **5**, 5362 (2014).

Supplementary Information is available in the online version of the paper.

Acknowledgements We thank T. Kueck for primary lymphocytes and S. Giese for assistance with smFISH. This work was supported NIH grants R01AI50111 and P50GM103297 (to P.D.B.)

Author Contributions M.A.T. performed all experiments unless otherwise stated and wrote the paper. D.G.-C. performed some of the luciferase reporter experiments and bioinformatic analyses. T.M.Z. performed smFISH experiments. A.Y. performed some of the CLIP experiments. D.B.-M. generated the mutant sequence *in silico*. S.J.S. constructed and characterized the 16 original mutant HIV-1 strains. P.D.B. conceived the study, supervised the work and wrote the paper.

Author Information Reprints and permissions information is available at www.nature.com/reprints. The authors declare no competing financial interests. Readers are welcome to comment on the online version of the paper. Publisher's note: Springer Nature remains neutral with regard to jurisdictional claims in published maps and institutional affiliations. Correspondence and requests for materials should be addressed to P.D.B. (pbeniasz@rockefeller.edu).

Reviewer Information *Nature* thanks G. Towers and the other anonymous reviewer(s) for their contribution to the peer review of this work.

METHODS

Plasmid constructs. A synonymously mutated HIV-1 sequence was designed that contained a maximum number of substitutions in open reading frames. Mutations were designed to maximize the probability of disrupting secondary structure by incorporating transversion mutations (purine to pyrimidine or vice versa) where possible. No new AG or GU dinucleotides were introduced, to avoid the creation of new splice acceptors and donors. Sequences encoding overlapping open reading frames were not altered, and all known *cis*-acting elements that control HIV-1 splicing, gene expression and other aspects of HIV-1 replication⁹ were intact in the mutant viral genome.

This designed HIV-1 sequence contained 1,976 synonymous mutations. It was divided into 150–500-nucleotide blocks (A–P), which were synthesized (Genewiz) and introduced in place of native sequence into HIV-1_{NHG}, a proviral plasmid containing a reporter GFP embedded in *nef*, or HIV-1_{NL4-3}, using restriction sites proximal to the mutated regions. Supplementary Data 1 contains a codon-by-codon list of the mutations made in segment L, and Supplementary Data 2 and 3 contain alignments of the wild-type and mutant EH and L segments (Fasta format). A complete characterization of the virus mutants not described in detail in this manuscript will be published elsewhere (M.T., S.J.S., D.B.M. and P.D.B.). Division (L, M) or combination (EH) of the original mutants blocks into derivative mutants was achieved using overlap extension PCR-based approaches with mutant and wild-type templates.

A ZAP exon 1-targeting guide sequence: 5'-GGCGGGATCACCGATCG GTGG-3' was inserted into a lentivirus-based CRISPR plasmid from Addgene (52961) to generate ZAP^{-/-} cells. A ZAP-S cDNA that was rendered resistant to CRISPR through introduction of synonymous mutations in the guide target sequence was generated by overlap extension PCR and inserted into a tetracycline-inducible HIV-1-based vector (pLKO.dCMV.TetO/R). An epitope-tagged (ZAP-3×HA) cDNA used for CLIP was inserted into the MLV expression vector, LHCX. A firefly luciferase cDNA (*fluc*) was designed to remove CG dinucleotides through synonymous substitution, reducing the total number of CG dinucleotides from 97 to 8. This CG-low *fluc* cDNA was inserted into the expression vector pCR3.1 using EcoRI and NotI. Various sequences were then inserted 3' to the *fluc* cDNA using NotI and XhoI. Specifically, sequences from the Indiana strain of VSV-G and -P and the influenza A/WSN/1933 NP ORFs were inserted, as were derivatives with synonymous mutations that maximized CG dinucleotide content. A CXCR4-2A-CD4 cassette was generated by overlap-extension PCR and inserted into LHCX using HindIII and HpaI.

Cells. The adherent cells 293T, HOS and HeLa were obtained from the ATCC and grown in DMEM with 10% fetal bovine serum. MT4 cells were obtained from the NIH AIDS reagent repository and cultured in RPMI supplemented with 10% fetal bovine serum. The identities of cell lines were routinely confirmed by visual inspection by an experienced scientist and cells were not routinely tested for mycoplasma contamination. Primary lymphocytes were isolated from human blood by Ficoll-Paque gradient centrifugation and removal of the plastic adherent fraction. Cells were activated with phytohaemagglutinin (Sigma, 5 µg ml⁻¹) and cultured in the presence of interleukin-2 (50 U ml⁻¹) in RPMI with 10% fetal bovine serum.

ZAP-deficient cells were generated by transduction with the lenti-CRISPR vector followed by selection in 5 µg ml⁻¹ blasticidin. Single-cell clones were derived by limiting dilution and maintained in the appropriate media with 5 µg ml⁻¹ blasticidin. Loss of ZAP protein and gene was confirmed by PCR amplification and sequencing the genomic locus and by western blotting. In some CRISPR knockout clones, protein species that reacted with an anti-ZAP antibody arose after extended passage; these are likely to represent truncated forms of ZAP-L whose translation initiated at methionine codons 3' to the CRISPR target site (near the ZAP N terminus). The appearance of these protein species did not affect the ability of the cells to support replication of wild-type or mutant viruses. Doxycycline-inducible ZAP-S expression in MT4 cells was reconstituted by stable transduction with the LKO ZAP-S expression vector followed by selection in 2.5 µg ml⁻¹ puromycin. These reconstituted cells were used as a pool. Cells (293T) stably expressing either ZAP-S-3×HA or ZAP-L-3×HA were generated by transduction with the LHCX vector containing the corresponding cDNA sequences followed by selection in 50 µg ml⁻¹ hygromycin. A single-cell clone was derived by limiting dilution and maintained in DMEM with 50 µg ml⁻¹ hygromycin. HOS cells were stably transduced with LHCX CXCR4-2A-CD4 followed by selection in 25 µg ml⁻¹ hygromycin. A single cell clone was derived by limiting dilution and maintained in the appropriate media with 25 µg ml⁻¹ hygromycin.

Viruses. All HIV-1 virus stocks were generated by transfection of 293T cells in 10-cm dishes with 10 µg proviral plasmid using polyethyleneimine (Polysciences). HIV-1_{WT} and mutant viruses usually contained a GFP reporter and were generated by transfection with HIV-1_{NHG}-derived proviral plasmids. The yields of infectious virus from transfected 293T cells for each of the mutants was similar, despite their differing properties in spreading replication assays. This is likely to be due to gross overexpression of the viral genome in transfected 293T cells. Viruses used

in primary lymphocyte replication and CLIP assays were generated by transfection with HIV-1_{NL4-3}. Viruses used to infect CD4-negative HeLa cells in the single cycle replication siRNA screen, or 293T cells in the CLIP assays, were generated by transfection with 10 µg proviral plasmid and 1 µg VSV-G expression plasmid. **Infection assays.** Titres of viral stocks were determined by performing threefold serial dilutions in a 96-well plate and infecting 5 × 10³ MT4 cells per well. At 16–18 h after infection, dextran sulfate was added to each well at a concentration of 50 µg ml⁻¹ to prevent reinfection by nascent virions. At 48 h after infection, cells were fixed in 4% PFA and enumerated by FACS analysis using a CyFlow Space cytometer (Partec) coupled to a Hypercyte Autosampler (Intelicyt).

For spreading replication assays with GFP reporter viruses, viral stocks generated from transfected 293T cells were adjusted to the same number of single cycle infectious units (determined on MT4 cells as described above). Thereafter, 2 × 10⁵ MT4 cells were infected at an MOI of 0.002 in 2 ml RPMI. Aliquots of infected cells were withdrawn each day and fixed in 4% PFA, and the proportion of infected cells was determined by FACS analysis of GFP expression. For spreading replication assays in PBMCs, cells were infected at an MOI of 0.001. At 18 h after infection, the cells were washed four times with PBS and cultured in RPMI with 50 U ml⁻¹ interleukin-2. Supernatants were collected every 24 h. Viral particle release was determined by measuring the reverse transcriptase activity with a PCR-based assay.

For single cycle replication, MT4 cells were infected at an MOI of 1.0 with HIV-1_{NHG}-derived viruses, washed three times with PBS 18 h after infection, and resuspended in RPMI with 50 µg ml⁻¹ dextran sulfate to prevent reinfection. At 48 h after infection, cells and supernatants were collected for analysis. Half of the cells were lysed in SDS sample buffer for western blot analysis and half allocated for RNA extraction and to determine levels of unspliced RNA as described below. The supernatants were filtered with a 0.22-µm filter. An aliquot of filtered supernatant was used to determine infectious viron yield by titration on MT4 cells. The remaining supernatant was centrifuged over a 20% sucrose cushion at 14,000 r.p.m. at 4 °C for 90 min. Pelleted virions were resuspended in SDS sample buffer for western blot analysis.

RT-qPCR analysis. RNA was collected from infected cells using the Nucleospin RNA kit (Macherey Nagel). The RNA concentration was determined using a NanoDrop 2000c (ThermoFisher). Equal amounts of RNA were reverse transcribed using SuperScript III reverse transcriptase with random hexamer priming (ThermoFisher). The cDNA was used as a template for quantitative real-time PCR using a StepOnePlus qPCR machine (Applied Biosystems). Unspliced viral RNA was detected by a TaqMan probe spanning the major splice donor D1, using the Fast Start TaqMan Probe master-mix. Serial tenfold dilutions of known copy numbers of HIV-1_{NHG} plasmid were used to generate a standard curve. The sequence of the TaqMan probe and primers were: D1 probe: 5'-GGCGGGCGACTGGTGAGT-3'; forward primer: 5'-GGACTTGAAAGCGAAAGGGA-3'; reverse primer: 5'-TCTCTCCTCTAGCCTCCG-3'.

Western blot analyses and antibodies. Cells were counted, normalized for cell number, lysed in SDS sample buffer, separated by electrophoresis on NuPage 4–12% Bis-Tris gels (Novex) and blotted onto nitrocellulose membranes (GE Healthcare). Antibodies against PTBP1 (ab5642), Drosha (ab12286), DICR (ab14601), EXOSC6 (ab50910), EXOSC10 (ab50558), and PARN (ab188333) were obtained from Abcam. Antibodies for Upf1 (A300-036A), METTL3 (A301-567A), EXOSC4 (A303-775A), EXOSC5 (A303-887A), and Xrn1 (A300-443A) were obtained from Bethyl Labs. The antibody against ZAP (16820-1-AP) was obtained from Proteintech. The HIV-1 capsid antibody (183-H12-5C) was obtained from the NIH AIDS reagent repository. The GFP (G1546) antibody was obtained from Sigma. The HIV Env (12-6205-1) antibody was obtained from American Research Products. The HA (HA.11) antibody used in the CLIP assays was obtained from Biolegend.

Single-molecule fluorescence *in situ* hybridization. HOS CXCR4-2A-CD4 were seeded onto gelatin-coated glass-bottomed 24-well plates (MatTek) and infected at an approximate MOI of <1 with HIV-1_{WT}, L_{CG-H1}, or L_{GC-H1}. Twenty-eight hours after infection the cells were washed with PBS and fixed with 4% paraformaldehyde (Thermo) in PBS for 30 min at room temperature. After permeabilization with 70% ethanol for 2 h at room temperature the cells were briefly washed with Stellaris RNA-FISH wash buffer A for 5 min at room temperature. The cells were then incubated with custom Stellaris smFISH probes targeting HIV-1 gag or all viral mRNAs (Biosearch Technologies) at a concentration of 0.125 µM in Stellaris RNA FISH hybridization buffer for 16–18 h at 37 °C. The cells were then washed twice for 30 min at 37 °C in Stellaris RNA FISH wash buffer A. The second wash contained Hoechst dye at 1 µg ml⁻¹. After a 5-min wash with Stellaris RNA FISH wash buffer B, cells were rinsed three times with PBS and imaged by deconvolution microscopy (Deltavision). Image stacks were generated by maximum intensity projection using the Z project function in ImageJ (Version 2.0.0-rc-59/1.51n). RNA spots were counted using Find Maxima function in ImageJ.

RNA interference screen. Cells were transfected with 50 pmol siRNA SMART pool (Dharmacon) using RNAiMAX (Thermo Fisher) in a 6-well plate seeded

with 2×10^5 HeLa cells per well. At 24 h after transfection, the cells were infected with either wild-type HIV-1_{NHG} or L_{CG-HI}. At 48 h after transfection, the cells were washed three times with PBS and suspended in DMEM. The cells and supernatant were collected 72 h after transfection to determine knockdown efficiency levels and the yield of infectious virions.

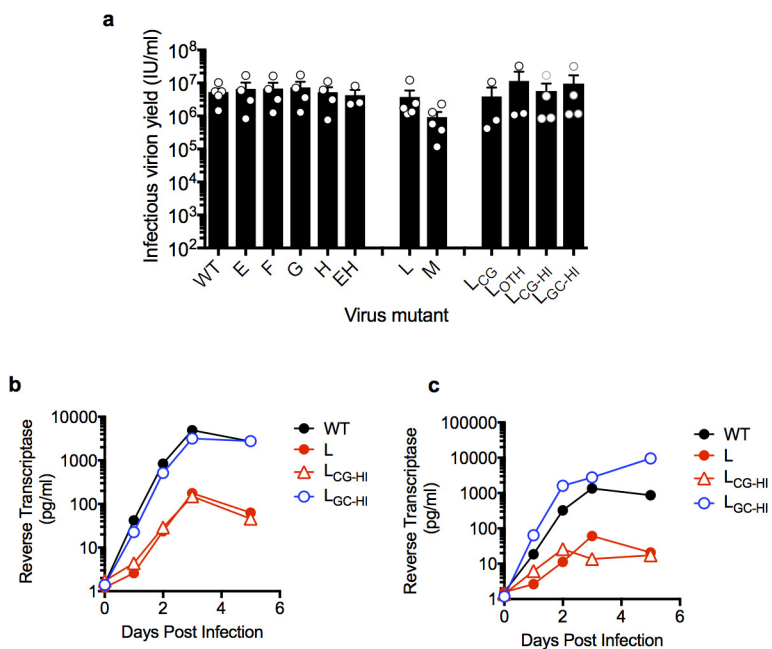
CLIP-seq. The CLIP method used in this study has been previously described²⁹. In brief, RNA and proteins were cross linked by feeding cells overnight with 4-thiouridine and irradiating them at 0.15 J cm^{-2} UV ($\lambda = 365 \text{ nm}$) in Stratalinker 2400 UV crosslinker (Stratagene). Thereafter, ZAP-3×HA was immunopurified using Protein G-conjugated magnetic Dynabeads and a mouse monoclonal anti-HA antibody, and the RNA was radiolabelled with $0.5 \mu\text{Ci} \mu\text{l}^{-1} \gamma\text{-}32\text{P}[\text{ATP}]$. Protein-RNA adducts were separated by SDS-PAGE, transferred to nitrocellulose and detected by autoradiography. Next, sequential 3' and 5' adaptor ligations were performed as previously described²⁹ by attaching a known sequence that contains primer binding sites for reverse transcription and PCR-amplification of the cDNA library. Sequencing of the cDNA library was done on an Illumina HiSeq 2000 platform.

The analysis pipeline used in this study has previously been described²⁹. Processing of raw reads was performed with the FASTX toolkit (http://hannonlab.cshl.edu/fastx_toolkit/), excluding reads with fewer than 15 nucleotides. Reads were then aligned to the human genome (hg38) concatenated with the HIV-1_{NL4-3} genome or to the viral genome alone. Cluster analysis was performed using PARalyzer³⁰.

Statistical information. HIV-1 replication experiments were done at least three times and representative data are shown. CLIP experiments were done four times and representative data are shown. Statistical analysis of smFISH data was done using the Mann–Whitney *U* test. Statistical analysis of variation in dinucleotide frequencies between ORFs, 3' UTRs and CLIP-derived ZAP-binding sequences and the human databases of ORFs and 3' UTRs were performed using Welch's unequal variance *t*-test implemented using R. All other experiments yielding quantitative data were done at least three times and mean values \pm s.e.m. are plotted. No statistical methods were used to predetermine sample size. The experiments were not randomized. The investigators were not blinded to allocation during experiments and outcome assessment.

Data availability. The sequence of the NHG proviral plasmid is available at Genbank (accession code JQ585717.1), as is the NHG-derived sequence containing all 12 mutant segments (accession code MF944225). The HIV-1 L mutant sequence has also been submitted to GenBank (accession code MF687717). The CLIP-seq data have been deposited in the NCBI GEO data repository with accession code GSE102843 (GSM2747099 and GSM2747100).

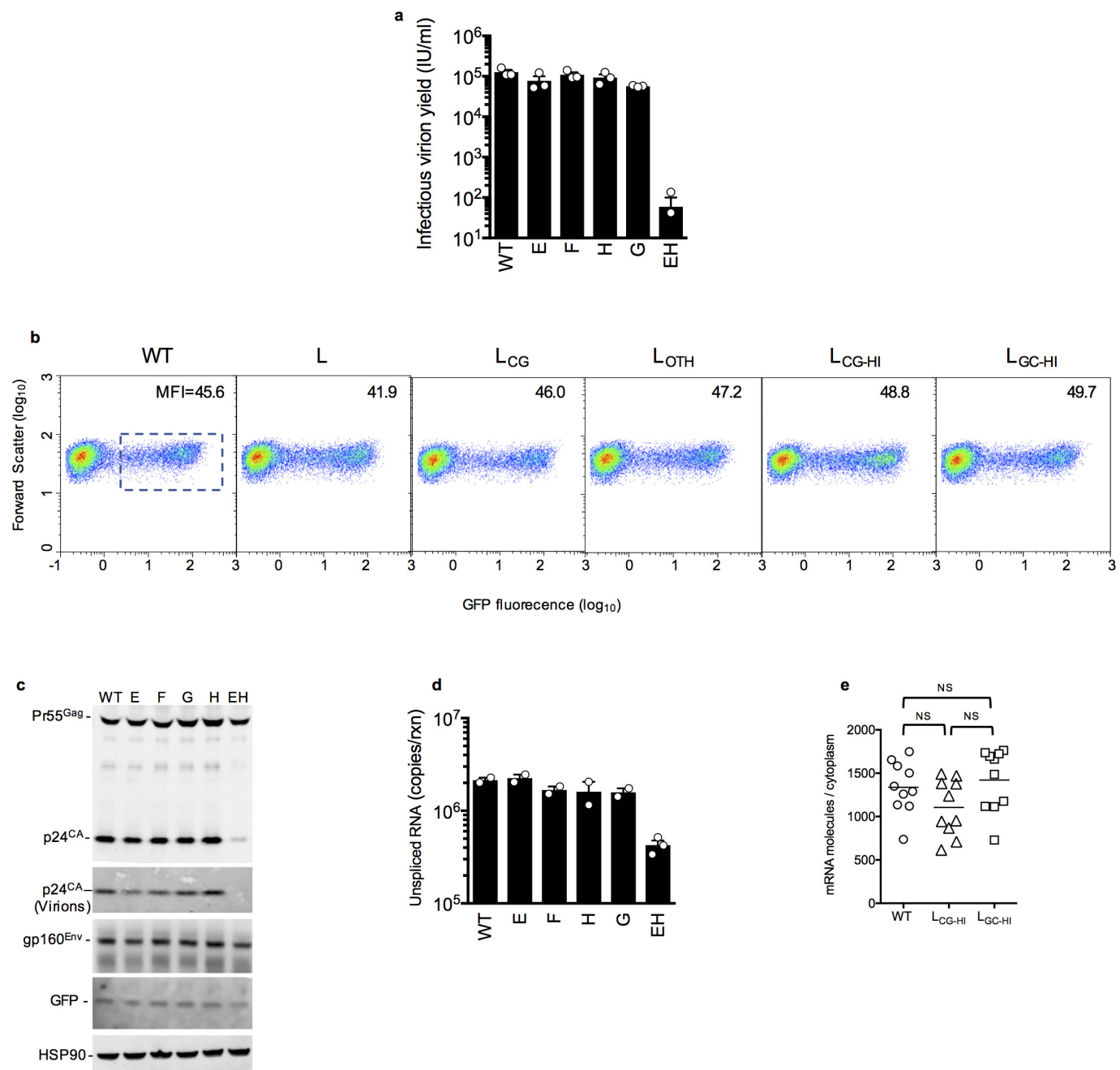
29. Kutluay, S. B. *et al.* Global changes in the RNA binding specificity of HIV-1 gag regulate virion genesis. *Cell* **159**, 1096–1109 (2014).
30. Corcoran, D. L. *et al.* PARalyzer: definition of RNA binding sites from PAR-CLIP short-read sequence data. *Genome Biol.* **12**, R79 (2011).



Extended Data Figure 1 | CG-enriched HIV-1 clones yield near wild-type levels of virus from transfected 293T cells but are attenuated in replication in primary lymphocytes. a, Yield of infectious virus from proviral plasmid transfected 293T cells, as measured by infection of

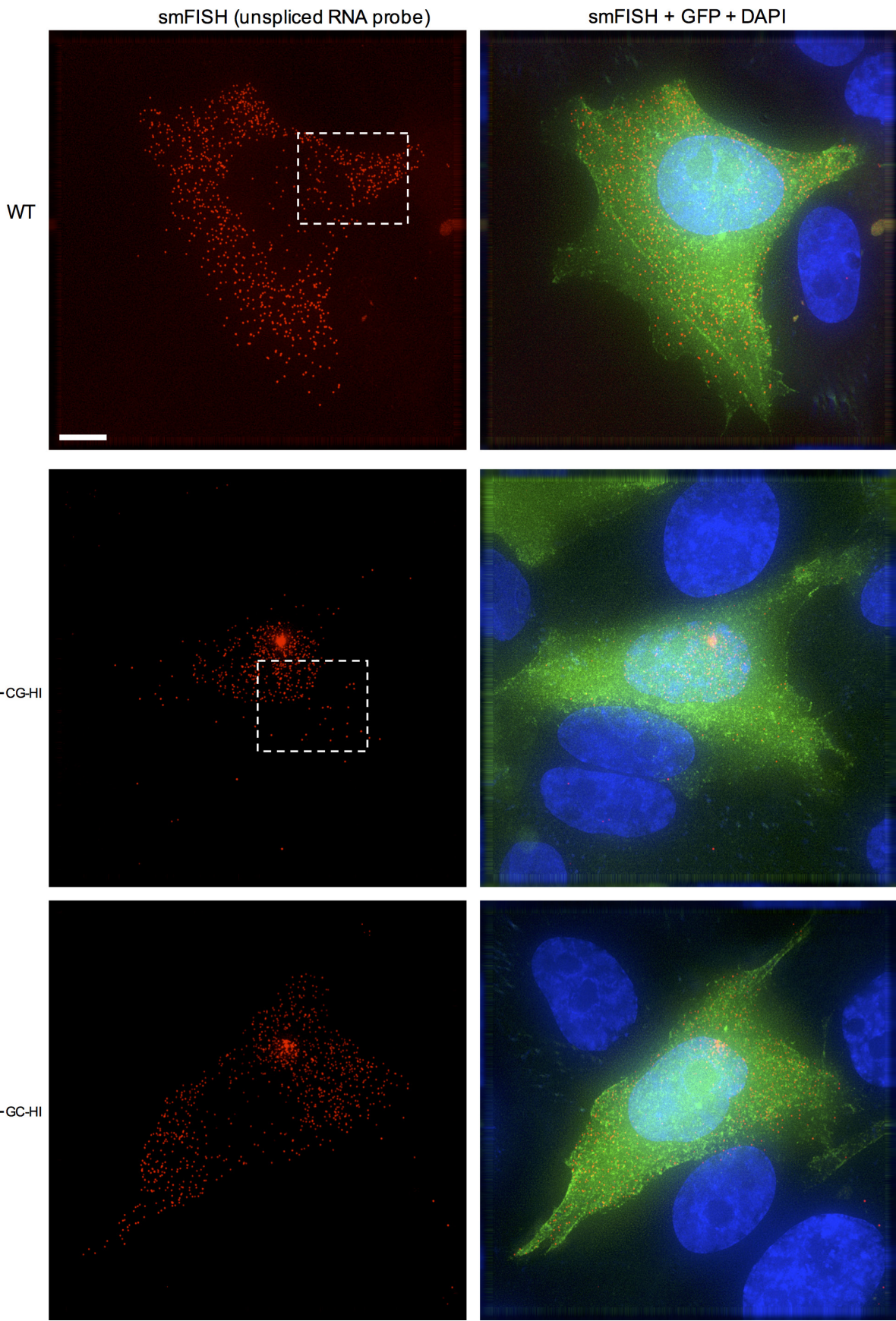
MT4 cells (mean \pm s.e.m., $n = 3, 4$ or 5 independent experiments).

b, c, Spreading replication of HIV-1 mutants in primary lymphocytes from two additional donors as measured by reverse transcriptase activity in the supernatant of infected cells over time.



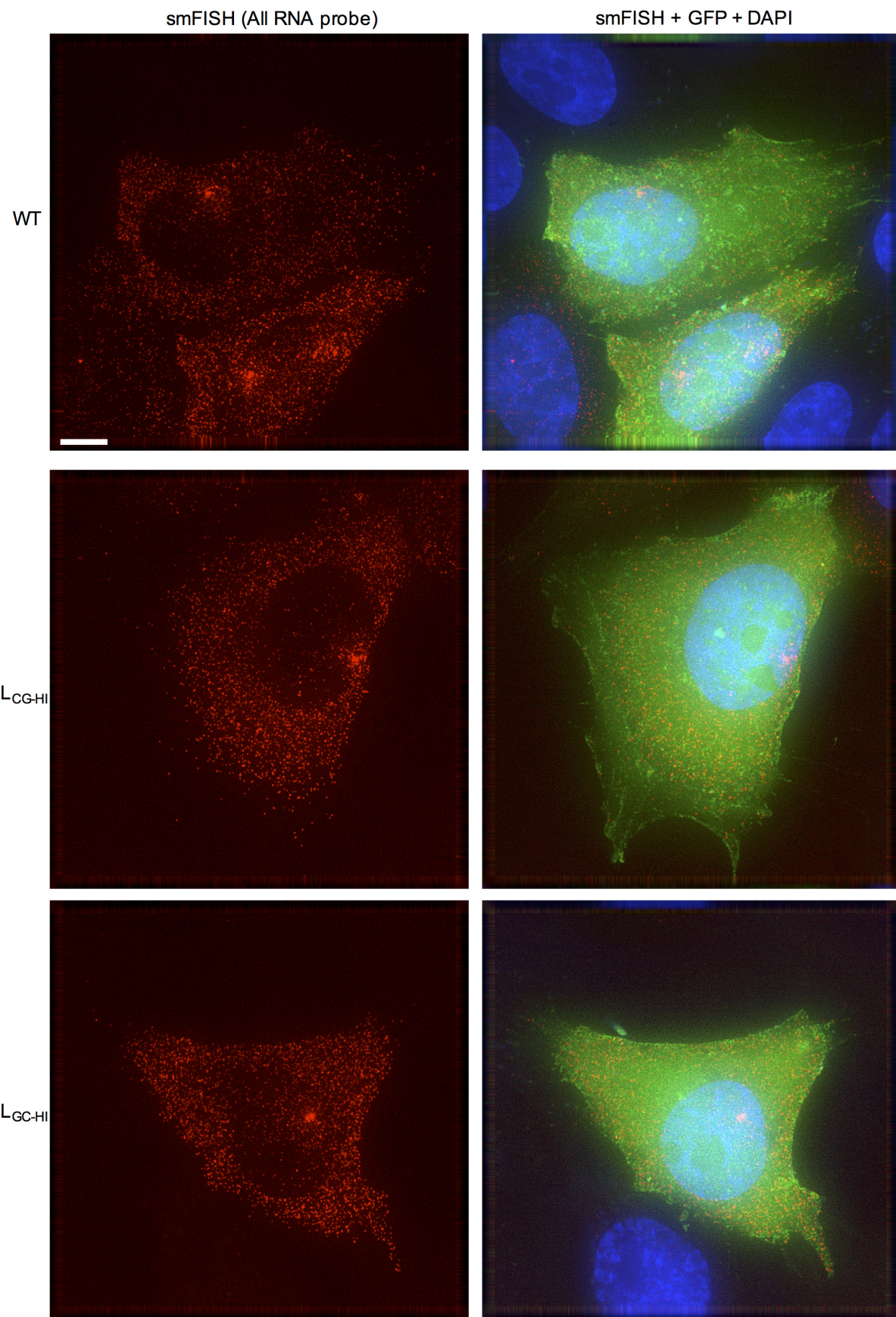
Extended Data Figure 2 | Effects of CG dinucleotides on HIV-1 infectious virion yield, RNA and protein levels in single-cycle replication assays. **a**, Yield of infectious virus in a single cycle of replication following infection of MT4 cells with equal titres of HIV-1_{WT} and *pol* mutants (mean ± s.e.m., $n = 3$ independent experiments). **b**, Expression of *gfp* in MT4 cells, as measured by flow cytometry, 48 h after infection with equal titres of the indicated viruses. Numerical values are mean fluorescent intensity (MFI) of infected cells (indicated by the dotted box). **c**, Western blot analysis (anti-Gag, anti-Env, anti-GFP and anti-HSP90) of viral, reporter and cellular protein

expression, 48 h after a single cycle of infection of MT4 cells with wild-type and synonymous *pol* mutant HIV-1. Representative of three experiments. **d**, RT-qPCR quantification of unspliced RNA in MT4 cells in a single-cycle infection assay with wild-type and synonymous *pol* mutant HIV-1 (mean ± s.e.m., $n = 2$ or 3 independent experiments). **e**, Quantification of RNA molecules (fluorescent spots) by smFISH in cytoplasm using a probe targeting all spliced and unspliced HIV-1 RNA species after infection of HOS/CXCR4-CD4 cells. Each symbol represents an individual cell. Horizontal lines represent mean values; P values were determined using Mann-Whitney test ($n = 10$).



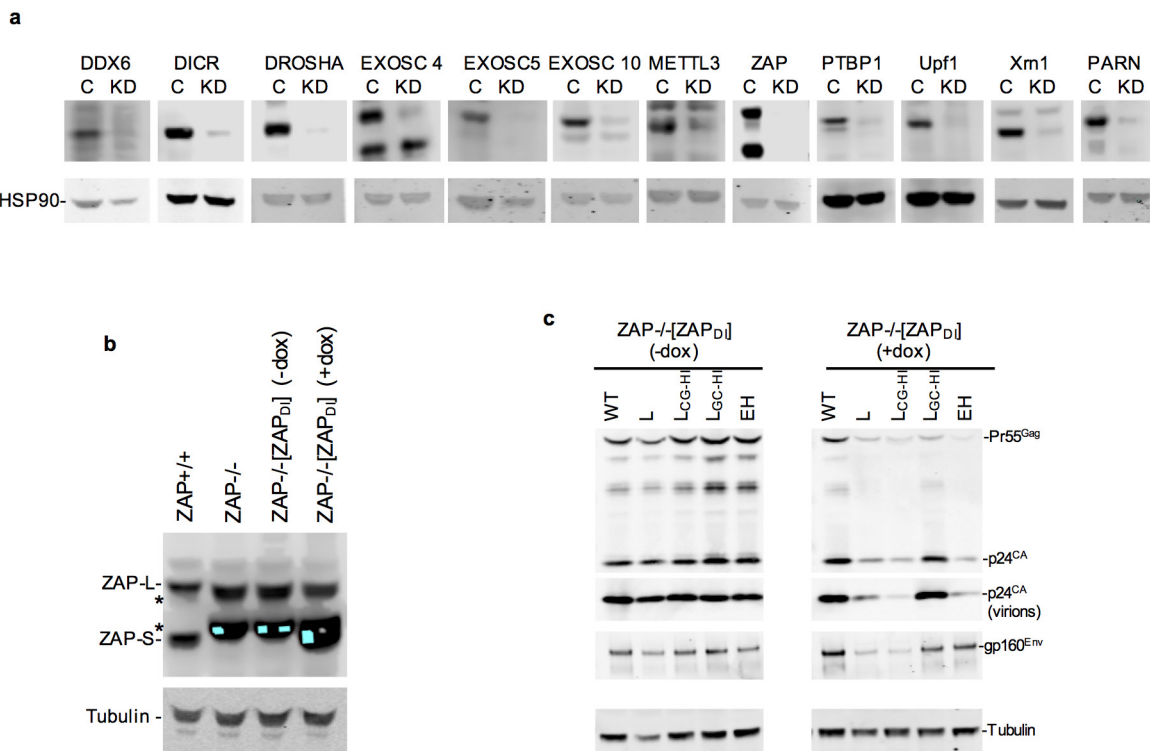
Extended Data Figure 3 | smFISH quantification of unspliced HIV-1 RNA in infected cells. Examples of smFISH analysis of wild-type and synonymous mutant HIV-1-infected cells (red, smFISH gag probe (see Fig. 2c); green, GFP; blue, Hoechst dye). The boxed areas indicate regions

selected for expanded views in Fig. 2f. Clusters of RNA molecules in the nuclei of some infected cells may represent sites of proviral integration. Representative of three independent experiments. Scale bar, 5 μ m.



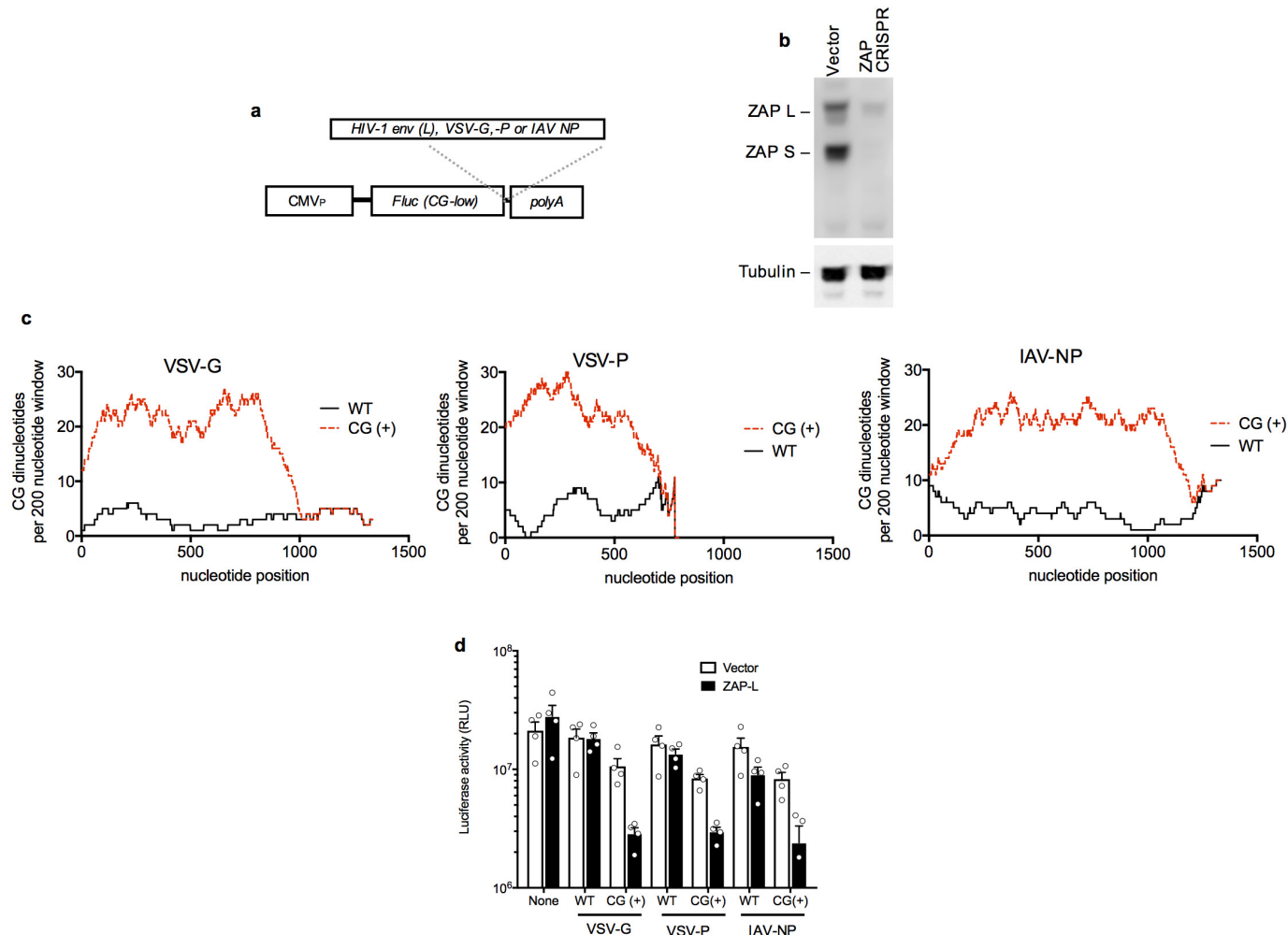
Extended Data Figure 4 | smFISH quantification of total HIV-1 RNA in infected cells. Examples of smFISH analysis of wild-type and synonymous mutant HIV-1-infected cells (red, smFISH probe targeting all viral mRNA species (see Fig. 2c); green, GFP; blue, Hoechst dye). Clusters of

RNA molecules in the nuclei of some infected cells may represent sites of proviral integration. Representative of three independent experiments. Scale bar, 5 μ m.



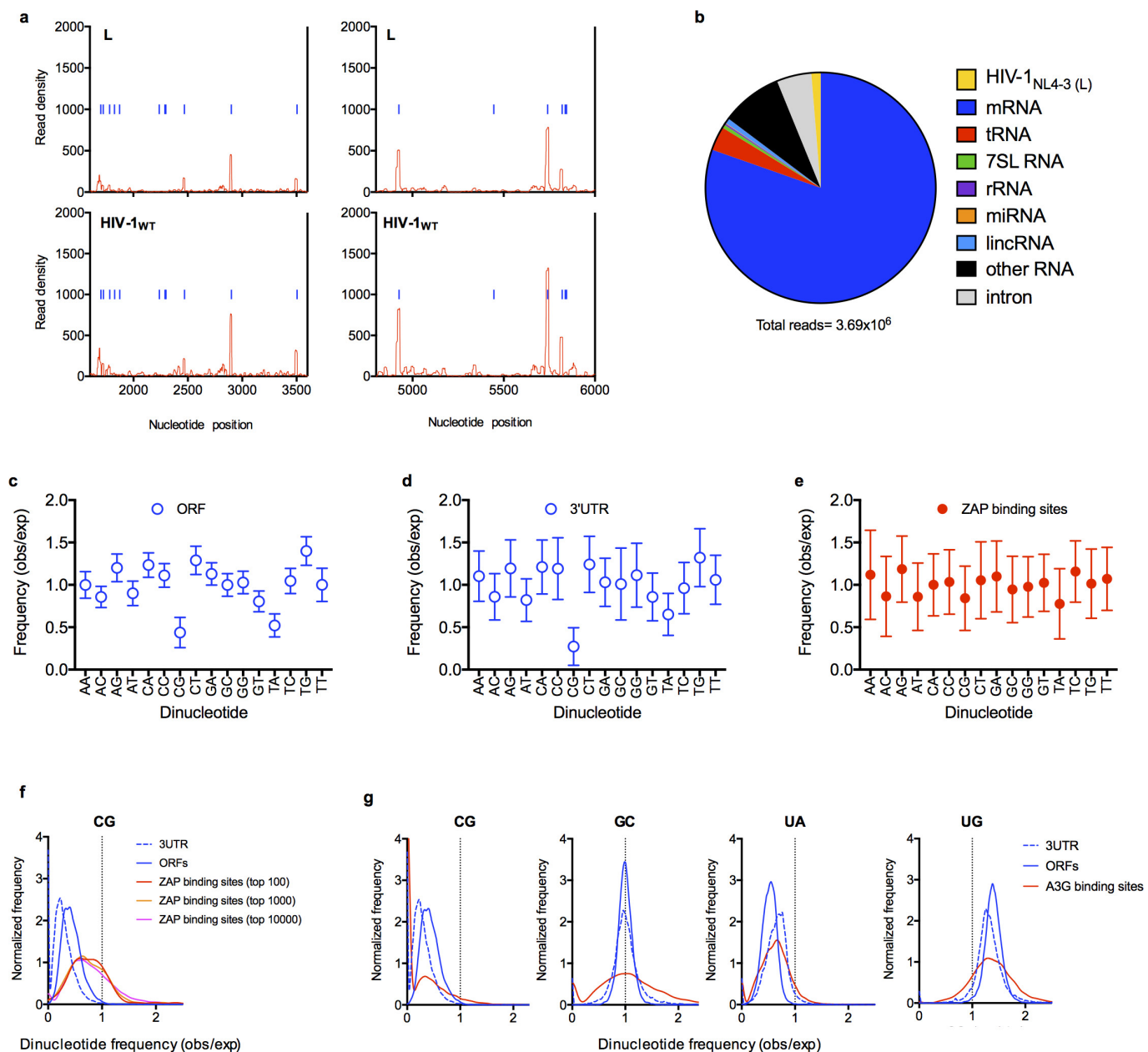
Extended Data Figure 5 | ZAP mediates deleterious effects of CG dinucleotides on HIV-1 replication. **a**, Western blot analyses, using the indicated antibodies, following transfection of HeLa cells with the corresponding siRNAs, or control siRNAs, in the single-cycle replication assays described in Fig. 3a. Representative of 2 experiments. **b**, Western blot analysis of ZAP expression in control, CRISPR-knockout MT4 cells and doxycycline-inducible ZAP-S-reconstituted MT4 cells. Asterisks indicate protein species that appeared in some CRISPR knockout clones, reacted with an anti-ZAP antibody and arose after extended passage.

These are likely to represent truncated forms of ZAP-L whose translation initiated at methionine codons 3' to the CRISPR target site (near the ZAP N terminus). Representative of three experiments. **c**, Western blot analysis (anti-Gag, anti-Env, anti-GFP and anti-tubulin) of viral and cellular protein levels in cells and virions, 48 h after single-cycle wild-type or mutant HIV-1 infection of ZAP^{-/-} MT4 cells that had been reconstituted with a doxycycline-inducible ZAP-S expression construct (ZAP_{D1}) and left untreated or treated with doxycycline. Representative of three experiments.



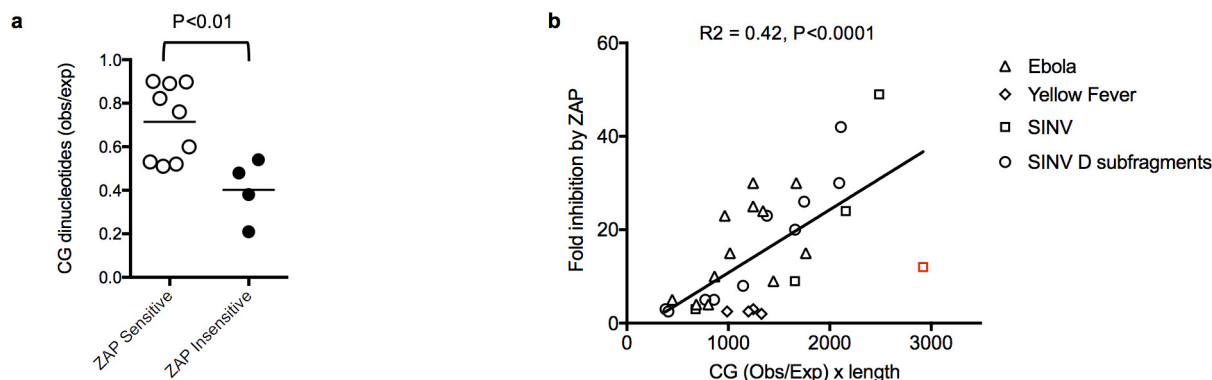
Extended Data Figure 6 | CG dinucleotides in 3' UTRs confer sensitivity to inhibition by ZAP. **a**, Schematic representation of a reporter construct encoding a CG dinucleotide-depleted *fluc* cDNA into which were inserted the indicated sequences as 3' UTRs. **b**, Western blot analysis of ZAP expression following CRISPR mutation of ZAP exon 1 in HeLa cells. Representative of three experiments. **c**, Number of CG dinucleotides present in a 200-nucleotide sliding window in the indicated

viral cDNA sequences that were left unmanipulated (WT) or recoded with synonymous mutations to contain the maximum number of CG dinucleotides (CG+). **d**, Luciferase expression following transfection of 293T ZAP^{-/-} cells with CG dinucleotide-depleted *fluc* reporter plasmids incorporating the indicated VSV or influenza A virus (IAV) RNA sequences as 3' UTRs, in the presence or absence of a cotransfected ZAP-L expression plasmid (mean ± s.e.m., $n = 4$ independent experiments).



Extended Data Figure 7 | **Dinucleotide composition of ORFs, 3' UTRs, and preferred ZAP binding sites in cellular mRNAs.** **a**, Expanded views of the portion of the CLIP graphs in Fig. 4a corresponding to unmutated portions of the viral genome. **b**, Sources of RNA reads bound to ZAP in a typical CLIP-seq experiment, done using HIV-1-infected cells. **c–e**, Ratio of the observed frequency to the expected frequency (obs/exp, based on mononucleotide composition) for each of the 16 possible dinucleotides, in ORFs (**c**), 3' UTR sequences (**d**) and the 100 sites in cellular mRNAs that were most frequently bound by ZAP, based on CLIP read numbers (**e**).

Plotted values are mean \pm s.d. of all ORFs ($n = 35,170$) and 3' UTRs ($n = 135,557$) in the respective libraries or the most preferred ZAP binding sites ($n = 100$). **f**, Frequency distributions of CG dinucleotide observed/expected frequencies in human ORFs, 3' UTRs and top 100, top 1,000 and top 10,000 ZAP-binding sites in CLIP experiments. The top 100, top 1,000 and top 10,000 ZAP-binding sites account for 6.7%, 18.9% and 46.7% of total reads. **g**, Frequency distributions of CG, GC, UA and UG dinucleotide observed/expected frequencies in human ORFs, 3' UTRs and the top 100 APOBEC3G-binding sites in CLIP assays.



Extended Data Figure 8 | Analysis of CG suppression in previously reported ZAP-sensitive and ZAP-resistant viruses and ZAP-sensitizing elements. **a**, CG suppression in RNA and reverse transcribing viruses previously reported to be ZAP sensitive ($n = 9$, open symbols) and ZAP resistant ($n = 4$, filled symbols)^{7,17–20}. The viruses included in the analysis and their degrees of CG suppression (CG observed/expected) are: ZAP-sensitive: Sinbis virus (0.90), Semliki forest virus (0.89), Venezuelan equine encephalitis virus (0.76), ebolavirus (0.60), hepatitis B virus (0.52), Moloney murine leukaemia virus (0.51), Marburg virus (0.53), alphavirus M1 (0.89), Ross river virus (0.82); ZAP-insensitive: HIV-1 (0.21), yellow fever virus (0.38), vesicular stomatitis virus (0.48), poliovirus (0.54). The P value was calculated using Student's t -test (two-sided, $n = 9$ ZAP-sensitive viruses and $n = 4$ ZAP-resistant viruses).

Influenza virus (CG obs/exp = 0.44), which has been reported to be ZAP-resistant owing to the presence of an antagonist²⁴ and ZAP-L-sensitizing via an entirely distinct protein interaction-based mechanism²³, was excluded from this analysis. **b**, Analysis of previous published data on ZAP inhibition of reporter gene expression. Each RNA element derived from the indicated RNA viruses was placed in a 3' UTR of a luciferase reporter plasmid and fold inhibition by coexpressed ZAP is plotted against the product of CG suppression (CG observed/expected) and length for each RNA element. A data point that is a quantitative outlier from the general trend (indicated in red) is from the Sinbis (SINV) genome, but is nevertheless included in the linear regression analysis. P value was calculated using the F -test (two-sided, $n = 32$ data points). Data are from refs 13 and 18.

Extended Data Table 1 | Mutations in the HIV-1 L mutant and its derivatives

Virus	Mutations	CG dinucleotides added	CG dinucleotides total	GC dinucleotides total
WT	none	0	2	18
L	145 synonymous mutations	37	39	25
L _{CG}	37 mutations (subset of L mutations that generate new CG dinucleotides)	37	39	27
L _{OTH}	108 mutations (subset of L mutations that do not generate new CG dinucleotides)	0	2	19
L _{CG-HI}	41 mutations	41	43	18
L _{GC-HI}	9 mutations	0	2	27

Life Sciences Reporting Summary

Nature Research wishes to improve the reproducibility of the work we publish. This form is published with all life science papers and is intended to promote consistency and transparency in reporting. All life sciences submissions use this form; while some list items might not apply to an individual manuscript, all fields must be completed for clarity.

For further information on the points included in this form, see [Reporting Life Sciences Research](#). For further information on Nature Research policies, including our [data availability policy](#), see [Authors & Referees](#) and the [Editorial Policy Checklist](#).

► Experimental design

1. Sample size

Describe how sample size was determined.

Sample sizes were determined based on the Authors' experience of what is necessary to generate a convincing and compelling result
Effect sizes in the experiments are such that any reasonable observer would conclude that the sample sizes employed in the manuscript are sufficient to support the conclusions

2. Data exclusions

Describe any data exclusions.

Some Q-RT-PCR data were excluded due to a PCR machine breakdown that was detected only after the experiment was completed. (trends were the same as those reported, but raw values were ~ 100-fold lower than those reported)

Some CLIP experiments with low read counts were excluded (see below)

3. Replication

Describe whether the experimental findings were reliably reproduced.

The findings in this paper were remarkably reproducible. Every experiment was performed multiple times with essentially the same result
One exception is CLIP (Figure 4) - This is an inherently complex, long experiment. Occasionally sample loss, or reagent deterioration can result in low read counts. On such occasions, the entire experiment is discarded and repeated. During the course of this study we noticed read counts were declining, so we replaced all reagents, which fixed the problem. The CLIP results shown in figure 4 have been obtained on multiple occasions and by two different operators. We are absolutely confident in their veracity

4. Randomization

Describe how samples/organisms/participants were allocated into experimental groups.

N/A

5. Blinding

Describe whether the investigators were blinded to group allocation during data collection and/or analysis.

No blinding was done in this study. Virtually all the data are quantitative, most measurements are made using a machine, and not easily subject to operator bias

Note: all studies involving animals and/or human research participants must disclose whether blinding and randomization were used.

6. Statistical parameters

For all figures and tables that use statistical methods, confirm that the following items are present in relevant figure legends (or the Methods section if additional space is needed).

n/a	Confirmed
<input type="checkbox"/>	<input checked="" type="checkbox"/> The <u>exact</u> sample size (n) for each experimental group/condition, given as a discrete number and unit of measurement (animals, litters, cultures, etc.)
<input type="checkbox"/>	<input checked="" type="checkbox"/> A description of how samples were collected, noting whether measurements were taken from distinct samples or whether the same sample was measured repeatedly.
<input type="checkbox"/>	<input checked="" type="checkbox"/> A statement indicating how many times each experiment was replicated
<input type="checkbox"/>	<input checked="" type="checkbox"/> The statistical test(s) used and whether they are one- or two-sided (note: only common tests should be described solely by name; more complex techniques should be described in the Methods section)
<input checked="" type="checkbox"/>	<input type="checkbox"/> A description of any assumptions or corrections, such as an adjustment for multiple comparisons
<input type="checkbox"/>	<input checked="" type="checkbox"/> The test results (e.g. p values) given as exact values whenever possible and with confidence intervals noted
<input type="checkbox"/>	<input checked="" type="checkbox"/> A summary of the descriptive statistics, including central tendency (e.g. median, mean) and variation (e.g. standard deviation, interquartile range)
<input type="checkbox"/>	<input checked="" type="checkbox"/> Clearly defined error bars

See the web collection on [statistics for biologists](#) for further resources and guidance.

► Software

Policy information about [availability of computer code](#)

7. Software

Describe the software used to analyze the data in this study.

PRISM and R were used for statistical analysis, SSE (<http://www.virus-evolution.org/Downloads/Software/>) was used for analysis and manipulation of dinucleotide content. Processing of raw reads in CLIP experiments was performed with the FASTX toolkit (http://hannonlab.cshl.edu/fastx_toolkit/). Cluster analysis was performed using PARalyzer
A simple custom Python script was used to count CG dinucleotides in a sliding window (Fig 1f), it is available on request

For all studies, we encourage code deposition in a community repository (e.g. GitHub). Authors must make computer code available to editors and reviewers upon request. The *Nature Methods* [guidance for providing algorithms and software for publication](#) may be useful for any submission.

► Materials and reagents

Policy information about [availability of materials](#)

8. Materials availability

Indicate whether there are restrictions on availability of unique materials or if these materials are only available for distribution by a for-profit company.

No restrictions other than UBMTA

9. Antibodies

Describe the antibodies used and how they were validated for use in the system under study (i.e. assay and species).

The following antibodies were validated through siRNA knockdown to confirm the specificity :

Antibody	Supplier	Cat #
PTBP1	Abcam	ab5642
Drosha	Abcam	ab12286
DICR	Abcam	ab14601
EXOSC6	Abcam	ab50910
EXOSC10	Abcam	ab50558
PARN	Abcam	ab188333
Upf1	Bethyl Labs	A300-036A
METTL3	Bethyl Labs	A301-567A
EXOSC4	Bethyl Labs	A303-775A
EXOSC5	Bethyl Labs	A303-887A
Xrn1	Bethyl Labs	A300-443A
ZAP	Proteintech	16820-1-AP

The following antibodies were validated in our laboratory using western blot assays on human cells (infected with HIV-1 where appropriate) and are cited in our labs previous publications:

Antibody	Supplier	Cat #
HIV-1 CA	NIH AIDS Repository	183-H12-5C
GFP	Sigma	G1546
HIV-1 gp120	American Research Products	12-6205-1
HA	Biolegend	HA.11
HSP90 Rabbit	Santa Cruz	SC-7947
HSP90 Mouse	Santa Cruz	SC-69703

10. Eukaryotic cell lines

- a. State the source of each eukaryotic cell line used.
- b. Describe the method of cell line authentication used.
- c. Report whether the cell lines were tested for mycoplasma contamination.
- d. If any of the cell lines used in the paper are listed in the database of commonly misidentified cell lines maintained by [ICLAC](#), provide a scientific rationale for their use.

ATCC (293T, HeLa, HOS) NIH AIDS Reagent repository (MT4)

Microscopic inspection (these cells are easily distinguished based on morphology)

No

N/A

► Animals and human research participants

Policy information about [studies involving animals](#); when reporting animal research, follow the [ARRIVE guidelines](#)

11. Description of research animals

Provide details on animals and/or animal-derived materials used in the study.

N/A

Policy information about [studies involving human research participants](#)

12. Description of human research participants

Describe the covariate-relevant population characteristics of the human research participants.

N/A